SAND 97-1216C
SAND--97-1216C
CONF-9709107--

MICROSTRUCTURE OF BULK AND ELECTRO-FORMED Ni IMPLANTED WITH Ti AND C

D. M. Follstaedt, S. M. Myers, J. A. Knapp, M. T. Dugger and T. A. Christenson

Sandia National Laboratories

Albuquerque, NM 87185-1056

RECEIVED
NOV 05 1997
OSTI

Abstract

The microstructure of high-purity Ni implanted with overlapping concentration profiles of Ti and C was examined with transmission electron microscopy. An amorphous phase forms at concentrations of 15-18 at.% Ti and 22 at.% C, while a two-phase alloy (amorphous + fcc Ni) forms for ≤ 16 at.% C. Electroformed layers with sub-micron fcc grains of Ni or $Ni_{80}Fe_{20}$ were also found to be amorphized by Ti + C implantation, a key requirement for applying this treatment to Ni-based micro-electromechanical systems to reduce their friction and wear.

Sandia is a multiprogram laboratory
operated by Sandia Corporation, a
Lockheed Martin Company, for the
United States Department of Energy
under contract DE-AC04-94AL85000.

DISTRIBUTION OF THIS DOCUMENT IS UNLIMITED

MASTER

SM2IB Gatlinburg, Sept 97 10/13/97

Introduction

Nickel is being used as a structural metal for a class of miniature machines termed micro-electromechanical systems (MEMS). Precision molds can be prepared by x-ray exposure of photoresist and can be filled by electroplating Ni alloys, producing mechanical components with dimensions from micrometers to millimeters (German process acronym: LIGA) [1,2]. These electroformed parts would have metal-metal sliding contacts in operating devices, and untreated Ni exhibits poor tribological properties due to adhesion between contacts. Thus a surface treatment that reduces friction and wear is needed to produce such miniature devices with good performance and extended lifetimes.

Past work has shown that the dual, overlapping implantations of Ti and C greatly reduce the friction and wear of Fe and steels [3-5]. Detailed investigations indicate that this improved tribological performance is directly related to an amorphous Fe-Ti-C phase formed on the implanted surface [6-8]. This phase was discovered to form within Fe [9,10] and more recently within Ni [11] when sufficient Ti and C are introduced during implantation.

We have examined Ni implanted with Ti + C to evaluate the treatment for improving the tribological performance of Ni-based MEMS components. Initial examination showed that the implanted layer is very strong and hard [12]. Our work has now been extended to account for variations of composition and microstructure with depth, and the treatment has been shown to reduce the friction and wear of Ni [13-15]. Here we discuss detailed microstructural examinations of the amorphous phase and its composition limits in Ni, and compare the results to similar studies in Fe. A composition of 15 at.% Ti and 22 at.% C implanted into pure Ni produces a fully amorphous alloy; lower C content results in a two-phase layer of amorphous +

fcc Ni. We also examine the microstructure of electroformed Ni and $Ni_{80}Fe_{20}$ and demonstrate that a similar hard amorphous layer forms when they are implanted with Ti and C.

Implanted Pure Ni

High purity Ni foil was annealed for 2 hours at 1373 K and then implanted at room temperature with $2x10^{17}$ Ti/cm^2 at 180 keV followed by $2x10^{17}$ C/cm^2 at 45 keV, as discussed in detail elsewhere [13]. This treatment was found by 6 MeV ^{4}He ion backscattering spectrometry at 164° [13] to produce overlapping Ti and C depth profiles as seen in Fig. 1, and produced the expected amorphous phase. The implanted layer was examined with TEM at 200 kV using specimens back-thinned by jet electro-polishing with a nitric acid solution. This method often produces large free-standing areas of the amorphous layer that allow thicker regions with the Ni substrate present and thinner areas with only the amorphous layer to be separately identified. In areas where the Ni substrate had been removed, small fcc Ni crystallites (10-40 nm across) having the crystal orientation of the original Ni grain were found within the amorphous layer. The crystallites appear as irregularly shaped dark areas in the bright-field micrograph of Fig. 2a. They retain the crystal orientation of the original Ni grain as seen by their spot diffraction pattern in Fig. 2b; the diffuse ring from the amorphous layer is also seen.

We suspected that this two-phase regime might be caused by insufficient C immediately below the surface, and implanted an additional $3x10^{16}$ C/cm^2 at the lower energy of 20 keV; the diffraction pattern from the free-standing layer of this alloy is seen in Fig. 2c to contain the diffuse ring but no spots from fcc Ni, indicating that the two-phase material had been eliminated. Additional low-intensity, sharp arcs are also seen whose atomic spacings are in fair agreement with hexagonal Ni_2O_3, which has apparently formed on the surface of the alloy. Since a surface layer with fcc Ni might adhere more strongly to a metal pin in sliding contact, an alloy with the additional C implantation at 20 keV was used for tribological studies on pure bulk Ni [13,14].

The implantation producing the two-phase alloy is of interest for nanoindentation studies [13,15] and offers the possibility to identify critical concentrations of the amorphous phase; we therefore examined it with cross-section TEM. In this case, the implanted Ni foil was glued on edge within a stack of Si slices, and a cross-section disk was extracted and thinned using metallographic polishing followed by ion milling. Figure 3a shows a bright-field cross-section image with the Ni matrix in diffraction contrast. Centered near 50-nm depth is a featureless zone of amorphous material. The two-phase layer with fcc Ni crystallites appearing as dark particles extends from the surface to 30-nm depth. Beneath the amorphous layer the large fcc Ni grain extends into the substrate, but the material from 80 - 180 nm shows more contrast due to a high density of dislocations formed by Ti and C ions penetrating beneath the amorphous layer.

Dark-field imaging confirmed the above phase assignments. In Fig. 3b, imaging with an (002) Ni spot illuminates the particles in the two-phase layer (0-30 nm). Detailed examination of Figs. 3a and 3b shows a thin (~6 nm) layer of fine grains at the specimen surface; we infer that this is nickel oxide. Figure 3c is a dark-field image formed with the diffuse ring to illuminate the amorphous phase, which appears as a fine "speckle" of white spots that show a complementary distribution to the fcc Ni. In Fig. 3c, the Ni crystallites in the two-phase layer appear as dark areas having no fine white spots . Using both plan-view and cross-section TEM images, we estimate that the Ni crystallites occupy ~20 vol.% of the two-phase layer.

All the images indicate three sublayers in the implanted layer: I - two phase (amorphous + fcc Ni), II - fully amorphous, and III - heavily dislocated Ni(Ti,C). These layers were assigned separate mechanical properties in finite-element modeling of the response of the implanted Ni to nanoindentation. It was clear from the modeling alone that three such layers were required, but their delineation with cross-section TEM allows their mechanical properties to be fitted accurately with simulations of the indentation force versus depth curve [14,15]. The amorphous phase in region II has exceptional mechanical properties, including a yield stress of 4.7 GPa.

The concentration profiles of Ti and C for the alloy of Fig. 3 are shown in Fig. 1, along with the depth boundaries of the fully amorphous layer (II). This layer has a composition of 15 at.% Ti and 22 at.% C, while the two-phase layer has 18 at.% Ti but only 16 at.% C. The minimum C concentration of the amorphous phase is thus between 16 at.% and 22 at.% for 15-18 at.% Ti. At the deeper side of the amorphous layer, the concentration of 10 at.% Ti and 14 at.% C is insufficient to form the amorphous phase. The minimum C concentration for this Ti concentration appears to be a bit higher for Ni than for Fe, for which ~10 at.% C appears adequate [16]. In other work, we have found that amorphous Ni-Ti-C can be produced by pulsed laser deposition and that ~20 at.% of each is needed [17], consistent with the implanted alloy examined here. The profiles in Fig. 1 show that implanted ions do penetrate into layer III (30 - 180 nm) to produce the high density of dislocations. The backscattering analysis also detects O and a small amount is found at the specimen surface, consistent with our detecting it with TEM.

We have interpreted the two-phase region as being due to insufficient C. Incomplete amorphization could also be due to other limitations such as inadequate transformation kinetics. The Monte Carlo program TRIM97 [18] was used to assess atomic displacements in this layer. For a dose of 1×10^{16} C/cm^2 at 45 keV, corresponding to the last 1/10-th of the C implantation, we obtain ~10 dpa. Thus there are sufficient displacements for fully amorphous material to have formed. Since adjacent layer II with increased C concentration is fully amorphous, we infer that the two-phase material is compositionally limited. Such a two-phase region was also found in Ti

+ C implanted Fe [9,10], and the composition is again believed to be insufficient for full amorphization [16]. Small Fe crystallites embedded in amorphous material but retaining the lattice orientation of the original crystalline matrix were observed [9], like those seen here for Ni.

Electroformed Ni alloys

Foils of electroformed Ni and $Ni_{80}Fe_{20}$ were examined before and after implantation of Ti + C. The Ni was electroplated to a thickness of 0.15 mm from a sulfamate bath at 50°C with a current density of 50 mA/cm^2; these plating conditions were chosen to reduce stress in the deposited materials. The $Ni_{80}Fe_{20}$ alloy was plated from a nickel-iron sulfate bath at 25°C and 10 mA/cm^2. The microstructure of the as-deposited Ni is seen in Fig. 4. The diffraction pattern in Fig. 4a shows rings indexing to fcc Ni; however, the rings are not uniform in intensity but have sections of increased intensity, indicating that the material has some texturing with preferred grain orientations. The grains are seen in the bright-field micrograph of Fig. 4b. Bright-field and dark-field images show that the material has a broad range of grain sizes: 30-600 nm.

The small grain size is likely responsible for the increased strength and hardness of electroformed Ni relative to pure Ni. A yield strength of 1.4 GPa was determined for electroformed Ni by nanoindentation and modeling [14], whereas the value for bulk Ni is 0.15 GPa. We find that after annealing the material is softer, and since it exhibits substantial grain growth with annealing [19], the high strength probably results from the small grain sizes.

The grains in the electroformed $Ni_{80}Fe_{20}$ alloy are smaller than those of Ni. The dark-field image in Fig. 5, obtained with the (111) and (200) fcc rings, shows grains as small as ~20 nm and some as large as 90 nm. This material was also found to have a high yield stress, 1.9 GPa [14].

Ion implantation of the electroformed Ni with $2x10^{17}$ Ti/cm^2 at 180 keV followed by $2x10^{17}$ C/cm^2 at 45 keV produced a fully amorphous surface layer. Figure 6 is a dark-field image obtained with the (220) fcc Ni ring. The thicker part of the area in the image shows illuminated fcc grains beneath the amorphous layer, while the material in the thinner area is fully amorphous and shows no crystalline material. This fully amorphous layer contrasts with the same implantation of high-purity Ni for which a partially amorphous layer was found just below the surface (Fig. 3). We infer that defects in the polycrystalline Ni and perhaps impurities introduced during electroplating extended the amorphous phase to the surface of this specimen in spite of the slightly lower implanted C concentration in region I. An amorphous layer was also found on the surface of electroformed $Ni_{80}Fe_{20}$ but showed evidence that some grains may not have been fully amorphized. This variation between materials probably indicates that the C concentration (16 at.%) just below the surface is almost sufficient for full amorphization; detailed variations of the material being treated then determine the final microstructure.

Discussion

The Fe-Ti-C and Ni-Ti-C ternary amorphous alloys are rather special microstructures. Amorphization occurs when the synthesis technique produces a metal with ~20 at.% each of Ti and C in solution while avoiding the precipitation of TiC. The fcc or bcc solution is unstable and the amorphous phase forms instead. Ion implantation and vapor-phase quenching by pulsed-laser deposition [17] meet these conditions. In early work with steels implanted with Ti +C, the improved tribological performance was associated with the presence of the amorphous phase on their wearing surface [6-8]. The high strength and hardness now being determined for this phase and the similar tribological performance of Ni when it is amorphized further indicate that the phase is directly responsible. Benefits have also been obtained when Co is implanted with Ti and an amorphous phase was observed [20]; we suggest that a hard amorphous Co-Ti-C phase is responsible.

A notable difference of the Ni alloy from that of Fe is that C does not appear to be incorporated at the surface during Ti implantation. If C were being incorporated as in Fe [9,10], the implanted Ni would be expected to be fully amorphous up to the surface with no two-phase alloy as in layer I since the C concentration would be highest just below the surface. Several differences could be responsible for this change in C incorporation. First, our implanter and vacuum system have been improved. Secondly, the (unenhanced) C diffusion rate in Fe was sufficient to account reasonably for the depth over which C was incorporated; since the diffusion rates of C in Ni are several orders of magnitude lower [21], reduced diffusion of C from the surface into Ni may inhibit its incorporation. Finally, carbonaceous molecules in the vacuum system could be less readily decomposed on the Ni surface for introduction into the implanted layer. Further study is needed to understand this difference between Ni and Fe.

References

1. E. W. Becker, W. Ehrfeld, P. Hagmann, A. Maner, D. Münchmeyer, Microelectron. Engr., **4** (1986) 35.
2. H. Guckel, K. J. Skrobis, J. Klein and T. R. Christenson, J. Vac. Sci. Technol., **A 12** (1994) 2559.
3. I. L. Singer, C. A. Carosella and J. R. Reed, Nucl. Inst. Meth., **182-183** (1981) 923.
4. L. E. Pope, F. G. Yost, D. M. Follstaedt, J. A. Knapp and S. T. Picraux, in K. C. Ludema (ed.) Wear of Materials 1983, ASME, New York, 1983, p. 280.
5. D. M. Follstaedt, J. A. Knapp and L. E. Pope, Mat. Res. Soc. Symp. Proc., **140** (1989) 133.
6. D. M. Follstaedt, F. G. Yost, L. E. Pope, S. T. Picraux and J. A. Knapp, Appl. Phys. Lett., **43** (1993) 358.
7. D. M. Follstaedt, F. G. Yost and L. E. Pope, Mat. Res. Soc. Symp. Proc., **27** (1984) 655.
8. D. M. Follstaedt, J. A. Knapp, L. E. Pope, F. G. Yost and S. T. Picraux, Appl. Phys. Lett., **45** (1984) 529.
9. J. A. Knapp, D. M. Follstaedt and S. T. Picraux, in C. M. Preece and J. K. Hirvonen (eds.) Ion Implantation Metallurgy, TMS-AIME, New York, 1980, p.152.

10. D. M. Follstaedt, J. A. Knapp and S. T. Picraux, Appl. Phys. Lett., **37** (1980) 330.

11. A. W. Mullendore, L. E. Pope, A. K. Hays, G. C. Nelson, C. R. Hills and B. G. Lefevre, Thin Solid Films, **186** (1990) 215.

12. S. M. Myers, D. M. Follstaedt, J. A. Knapp and T. R. Christenson, Mat. Res. Soc. Symp. Proc., **444** (1997) 99.

13. S. M. Myers, J. A. Knapp, D. M. Follstaedt and M. T. Dugger, submitted to Journal of Applied Physics.

14. S. M. Myers, J. A. Knapp, D. M. Follstaedt, M. T. Dugger and T. R. Christenson, these proceedings.

15. J. A. Knapp, D. M. Follstaedt, S. M. Myers, J. C. Barbour, T. A. Friedmann, J. Ager, O. Monteiro and I. Brown, these proceedings.

16. J. A. Knapp, D. M. Follstaedt and B. L. Doyle, Nucl. Inst. Meth., **B 7/8** (1985) 38.

17. J. A. Knapp, D. M. Follstaedt and S. M. Myers, unpublished.

18. J. F. Ziegler, J. P. Biersack and U. Littmark, The Stopping and Range of Ions in Solids Pergamon, New York, 1985.

19. H. Guckel, T. R. Christenson, K. J. Skrobis, J. Klein and M. Karnowsky, Proc. "Transducers 1993" (Yokohama, Japan, June 7-10, 1993), p. 76.

20. S. A. Dillich, R. N. Bolster and I. L. Singer, Mat. Res. Soc. Symp. Proc., **27** (1984) 673.

21. Landolt-Börnstein Numerical Data and Functional Relationships in Science and Technology, Vol 26 "Diffusion in Solid Metals and Alloys", H. Mehrer (ed.), Springer-Verlag, Berlin, 1990, pp. 482, 498.

Figure Captions

Figure 1. Concentration profiles of Ti, C, and O in Ni implanted with $2x10^{17}$ Ti/cm^2 at 180 keV followed by $2x10^{17}$ C/cm^2 at 45 keV. The fully amorphous layer (II) is shaded, and C concentrations at the interface with the two-phase layer (I) are indicated.

Figure 2. a) Bright-field, plan-view TEM image of Ni implanted with $2x10^{17}$ Ti/cm^2 at 180 keV followed by $2x10^{17}$ C/cm^2 at 45 keV, showing Ni crystallites 10-30 nm across within the amorphous layer. b) Electron diffraction pattern from the layer in a) showing the diffuse ring from the amorphous phase and a fcc Ni spot pattern from the oriented crystallites. c) Diffuse ring from the amorphous phase of a layer implanted as above but with an additional $3x10^{16}$ C/cm^2 at 20 keV. Weak reflections from Ni oxide are indicated with arrows.

Figure 3. a) Bright-field, cross-section TEM image of Ni implanted with $2x10^{17}$ Ti/cm^2 at 180 keV followed by $2x10^{17}$ C/cm^2 at 45 keV, with the fcc Ni in diffraction contrast. The amorphous phase appears featureless in layer II (30-80 nm), but in layer I (0-30 nm) the Ni crystallites are observed. Beneath the amorphous layer, the Ni shows a high density of dislocations in layer III (80-180 nm). b) Dark-field image (enlarged) with fcc Ni illuminated. A thin layer of fine-grained oxide appears at the surface (between arrows). c) Corresponding dark-field image obtained with the diffuse ring; amorphous material is illuminated with a "speckle" of fine white spots. The Ni crystallites in layer I appear as dark areas.

Figure 4. TEM evaluation of electroformed Ni. a) Electron diffraction pattern showing rings from fcc Ni grains. b) Bright-field image of grains.

Figure 5. Dark-field TEM image of fcc grains in electroformed $Ni_{80}Fe_{20}$.

Figure 6. Dark-field TEM image of Ni implanted with $2x10^{17}$ Ti/cm^2 at 180 keV followed by $2x10^{17}$ C/cm^2 at 45 keV formed with (111) and (200) fcc reflections. Ni grains are illuminated in the thicker part of the area imaged, but are absent in the thinner area which is fully amorphous.

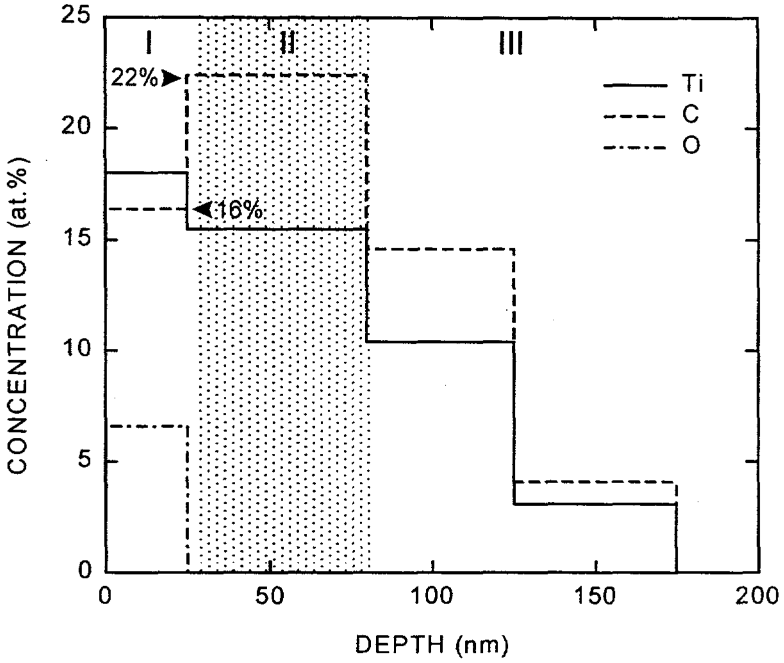

Follstaedt et al.

Figure 1

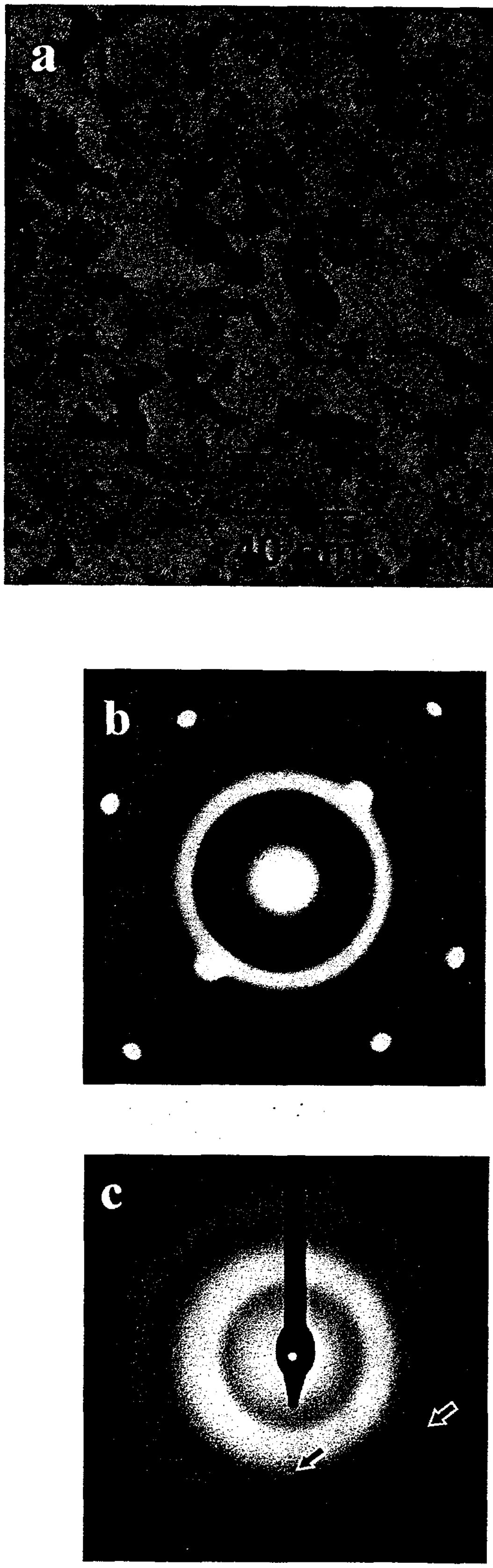

Follstaedt et al.

Figure 2

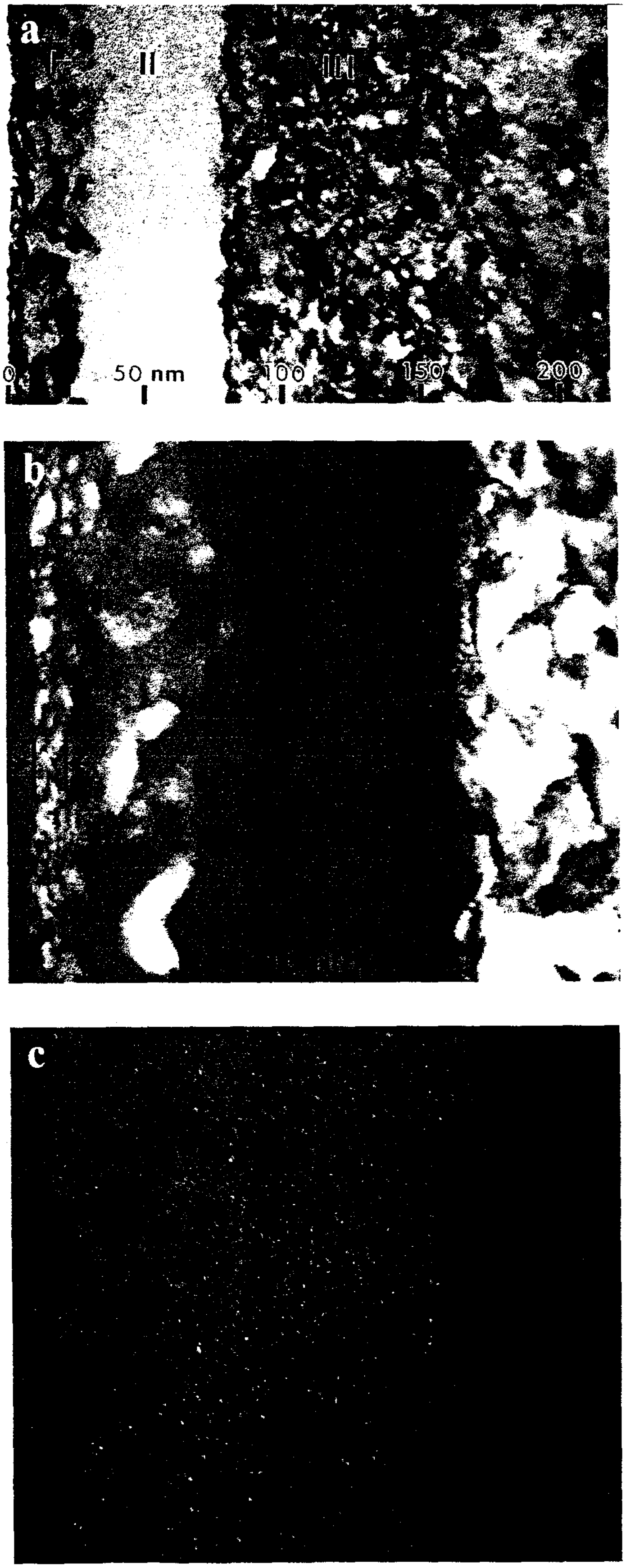

Figure 3

Follstaedt et al.

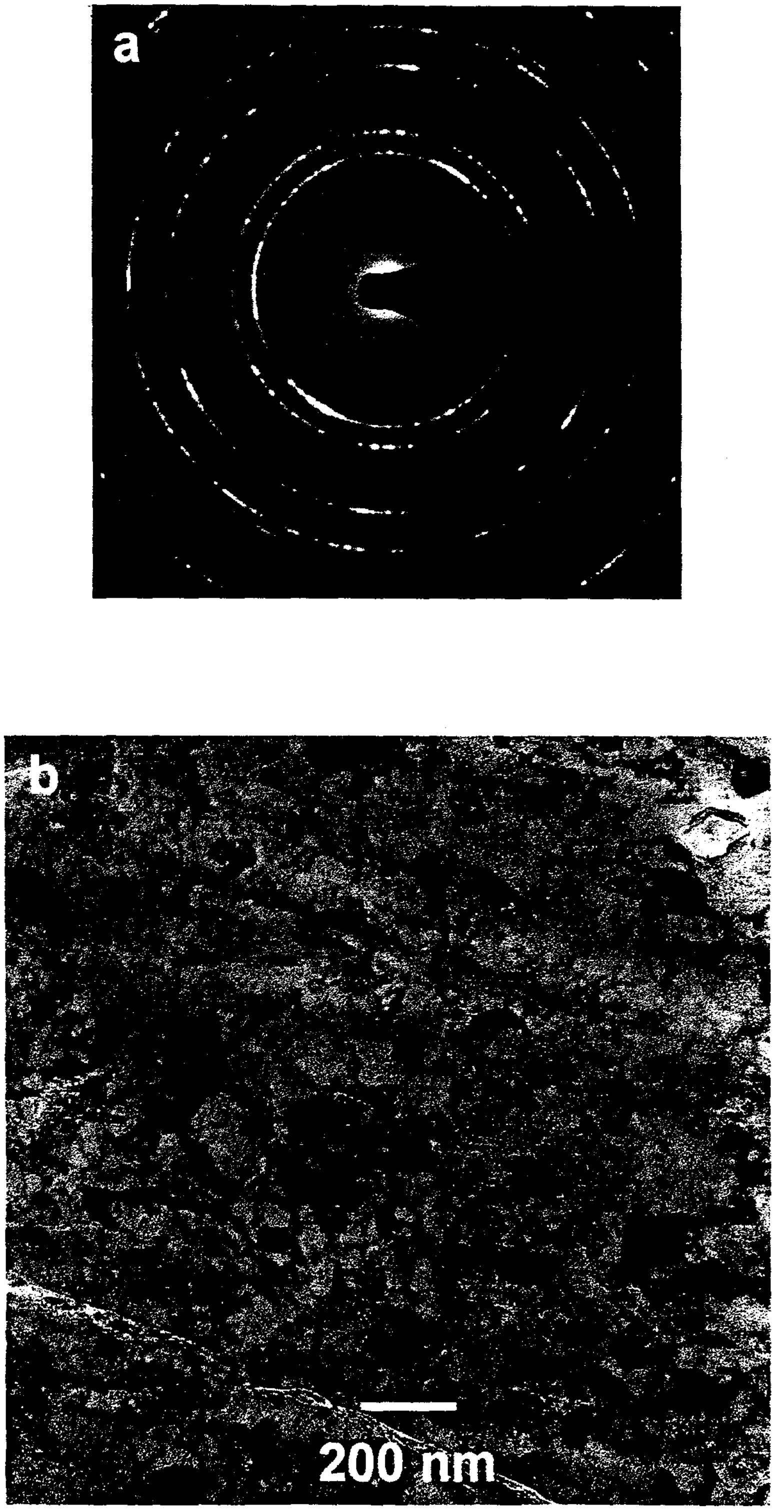

Follstaedt et al.

Figure 4

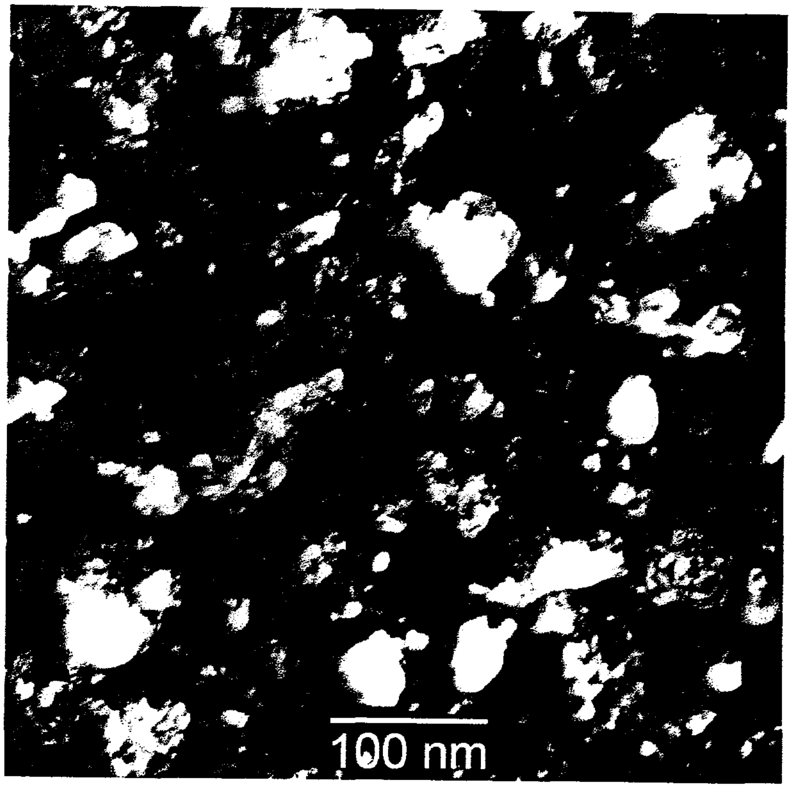

Follstaedt et al.

Figure 5

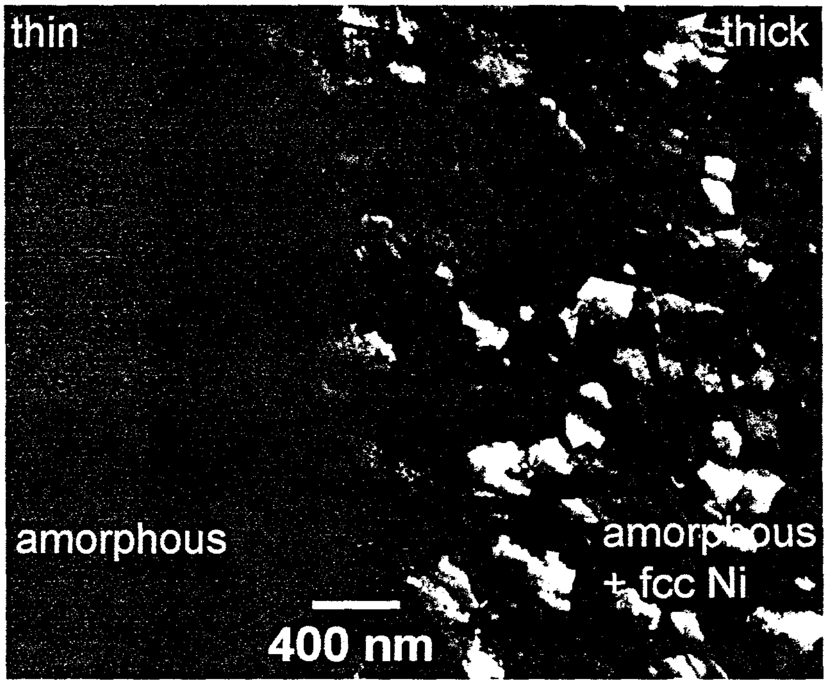

Follstaedt et al.

Figure 6